THE JOURNAL OF PHYSICAL CHEMISTRY C
A JOURNAL OF THE AMERICAN CHEMICAL SOCIETY

pubs.acs.org/JPCC

Perspective

Symmetry-Reduced Metal Nanostructures Offer New Opportunities in Plasmonics and Catalysis

Zachary J. Woessner and Sara E. Skrabalak*

Cite This: *J. Phys. Chem. C* 2021, 125, 23587–23596

Read Online

ACCESS | Metrics & More | Article Recommendations

ABSTRACT: Metallic nanoparticles (NPs) display interesting optical and catalytic properties that depend on NP composition, size, shape, and architecture. These NPs and their properties are often defined by the symmetry of the NPs themselves, with many seed-mediated syntheses for metal NPs maintaining the same symmetry between the seed and the resulting NP. However, recent research has shown that the symmetry of NPs can be reduced in a defined manner during seed-mediated syntheses through judicious control of reaction conditions. This ability offers unique and tunable optoelectronic and catalytic properties. In this Perspective, we outline general pathways to obtain NPs with reduced symmetry by seed-mediated methods and the interesting optical and catalytic properties that result from such a reduction in symmetry.

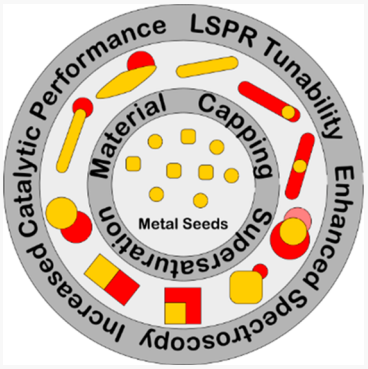

INTRODUCTION

Nanoscale materials provide unique and tailorable properties, giving rise to their use as theranostics and in applications such as chemical sensing and catalysis.[1−8] These applications depend heavily on the composition, size, shape, and architecture of the nanoscale crystals, with a desire for nanoscale multifunctional platforms driving a push for compositional and architectural complexity.[9] Traditionally, solution-derived nanoparticles (NPs) adopt shapes with high symmetry, *e.g.*, I_h or O_h symmetry, as these shapes can be viewed as thermodynamically preferred.[10,11] However, nature has shown that many critical processes such as cellular reproduction and cellular maturation arise from a reduction in symmetry.[12] Likewise, NPs with comparatively reduced symmetry often have markedly different properties when compared to their higher symmetry counterparts. Such differences are immediately evident when considering the optical properties of Au NPs of a quasi-spherical shape, which we can define as high symmetry, *i.e.*, D_∞, I_h, and O_h (aspect ratio = 1), and Au nanorods with dihedral symmetry *i.e.*, D_{nh} (aspect ratio >1). Spherical Au NPs exhibit a single, dipolar plasmon resonance.[1,3] In contrast, Au nanorods exhibit both a transverse and a longitudinal plasmon resonance consistent with the short and long axes of the nanorods.[13,14] A key feature is that these symmetry-reduced nanorods still can be defined by a set of symmetry operations; otherwise, their properties cannot be easily and reproducibly defined. Other examples have shown the efficacy of reduced-symmetry NPs with distinct domains such as heterodimers in achieving enhanced and tunable properties over their more symmetric counterparts.[15−19]

Seed-mediated methods are a premier route to NPs as monodisperse samples. With this technique, preformed NPs of a defined symmetry serve as preferential sites for additional deposition of material, as the barrier for heterogeneous nucleation (seeded) is lower than that of homogeneous nucleation.[10,20] On account of this benefit, new NPs with reduced symmetry relative to the initial NP seeds are being synthesized by seed-mediated methods.[21,22] Although a hallmark of seed-mediated methods has been symmetry transfer from seed to final NP,[23−25] controlled symmetry reduction has been achieved in enough systems such that general trends are emerging.[21] Typically, symmetry reduction is achieved during seed-mediated methods where there is a large lattice mismatch between the seeds and depositing material, the supply of depositing atoms is low (i.e., low supersaturation), nanocrystal surfaces (or seeds) are asymmetrically passivated, or seeds are confined at interfaces.[21] Symmetry-reduced NPs prepared by these methods are proving useful for applications ranging from security devices to electrocatalysts.[26−28]

Received: September 1, 2021
Revised: October 5, 2021
Published: October 21, 2021

https://doi.org/10.1021/acs.jpcc.1c07743
J. Phys. Chem. C 2021, 125, 23587–23596

In this Perspective, methods that promote growth of NPs with reduced symmetry via seed-mediated methods are emphasized, followed by a discussion of the properties and applications of symmetry-reduced metal NPs. While many of the synthetic principles extend across material classes, the emphasis on metal NPs arises from the confinement of electrons at the nanoscale and the facile control over NP size and shape leading to unique and interesting optoelectronic properties. The plasmonic properties that arise from good plasmonic materials, such as Au NPs, with defined symmetries will be highlighted to emphasize the ability to tune far- and near-field optoelectronic properties. From this foundation, we then discuss the use of symmetry-reduced NPs for tandem catalysis and photocatalysis. Although there are many excellent examples to select from as part of this discussion, we focused on symmetry-reduced NPs for CO_2 reduction given both current technological emphasis and the availability of studies that consider NP composition, size, and shape within one process. This focus also provides a natural transition to discuss hybrid NPs as an exciting frontier for this work. The Perspective concludes with current challenges in the synthesis of symmetry-reduced NPs that could open up new opportunities if addressed.

SYMMETRY-REDUCED NPS

The unique properties gained from introducing anisotropic features through a reduction in NP symmetry drives the need for robust synthetic methods; however, the current understanding of how to achieve structures with reduced symmetry by solution-phase methods restricts most routes to seed-mediated methods. Seed-mediated growth uses preformed NPs in which, under specific synthetic conditions, additional material (*e.g.*, more of the same material or a different material) is grown from the seed due to the lower energy barrier for heterogeneous nucleation compared to homogeneous nucleation.[10] For example, Au nanorods can be synthesized in high yields using seed-mediated growth methods. These methods typically use quasi-spherical, single-crystalline (cuboctahedra) Au seeds (O_h symmetry) in an aqueous solution of hexadecyltrimethylammonium bromide (CTAB) and small amounts of Ag^+ to induce anisotropic growth.[29] The asymmetric passivation of seeds promotes growth on certain parts of the seeds while others become more strongly passivated by Ag, promoting the 1D growth observed in nanorod formation (Figure 1A).[29,30] Overgrowth of a second material on a metal seed can introduce compositional and architectural complexity inherent to the spatial relationship between the seed and depositing material.[6] For example, rodlike particles have an additional degree of tunability by modifying the position of the metal seed in the interior of the resulting nanorod upon deposition of a secondary material, *i.e.*, centrosymmetric versus noncentrosymmetric (Figure 1B).[31] Additionally, asymmetric passivation can be achieved through controllably coating part of a seed with an unreactive protecting group such as collapsed polymer or silica and growing a secondary material on the exposed metal surface.[21,22,32−35] Polymers on NP seeds have promoted formation of NPs with nanogaps and chirality through seed-mediated growth.[36,37]

Manipulation of supersaturation during seeded growth can also produce symmetry-reduced NPs, with capping agent concentration often a contributing variable.[38] Manipulating these two factors leads to a changed energy barrier for heterogeneous nucleation, where low supersaturation and strong surface passivation leads to a higher energy barrier for heterogeneous nucleation and thus a lower rate of nucleation.[39] The intertwined relationship between supersaturation and surface passivation was shown experimentally by codepositing Au and Pd on Pd NPs of defined symmetry under varying metal precursor and capping agent concentrations.[39] Using low supersaturation and strong surface passivation conditions, asymmetric, vertex-driven overgrowth of Au-rich Au−Pd regions on Pd seeds of multiple shapes was observed.[39] The limited supply of atoms implied through low supersaturation allows for deposition to occur on some vertices but not every vertex, leading to a controllable reduction of the seed symmetry (Figure 1C).[39] Interestingly, in a second example where the supply of atoms was limited through the injection rate (*i.e.*, low supersaturation conditions), Ag deposited on only a single face of cubic Pd seeds, forming heterodimers with approximate C_{4v} symmetry, including NP composition in the assignment of symmetry.[40] Throughout this Perspective, the symmetry assignment will take both the NP shape and composition into account. We note that the supply of adatoms can also be limited to specific parts of the NP surfaces through immobilization of NP seeds at liquid−liquid and solid−liquid interfaces, inhibiting growth on the parts of the NPs blocked by the interface; these methods have yielded a variety of NP structures such as Janus-like heterodimers and nanocups.[21,41−45]

Heterodimers, structures where two phases are both exposed at the surface and connected via an interface are also of great interest. In addition to manipulation of supersaturation and asymmetric passivation of nanocrystal seeds, symmetry reduction can be achieved when there is a large lattice mismatch between the seed and depositing material (Figure 1D).[21] The large lattice mismatch between the seed and secondary metal leads to a lattice distortion at the interface between the two, leading to strain, which if energetically costly enough can lead to a change in growth mode.[21] To relieve the interfacial strain, metal adatoms will tend to adopt sites where the same material has already nucleated, leading to asymmetric growth. This type of growth mode is illustrated through the growth of Cu on Pd cubes (lattice mismatch of 7.1%) where the excessive strain leads to asymmetric growth, with an overall reduction of symmetry from O_h to approximately C_{4v} or lower.[46] Further, heterodimers can be used as templates toward more complex structures via subsequent growth steps.

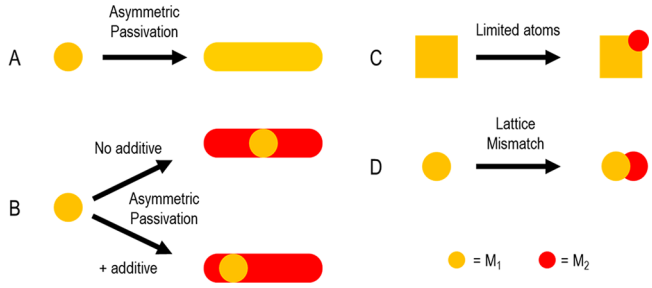

Figure 1. General strategies for promoting symmetry reduction during seeded growth with yellow representing a different metal than red. Schemes for (A) monometallic and (B) bimetallic nanorod syntheses in seeded systems where additives can manipulate the location of the seed in the resulting particles. (C) General route toward site-specific deposition using limited-atom supply and (D) route toward heterodimer formation through using lattice mismatch.

https://doi.org/10.1021/acs.jpcc.1c07743
J. Phys. Chem. C 2021, 125, 23587−23596

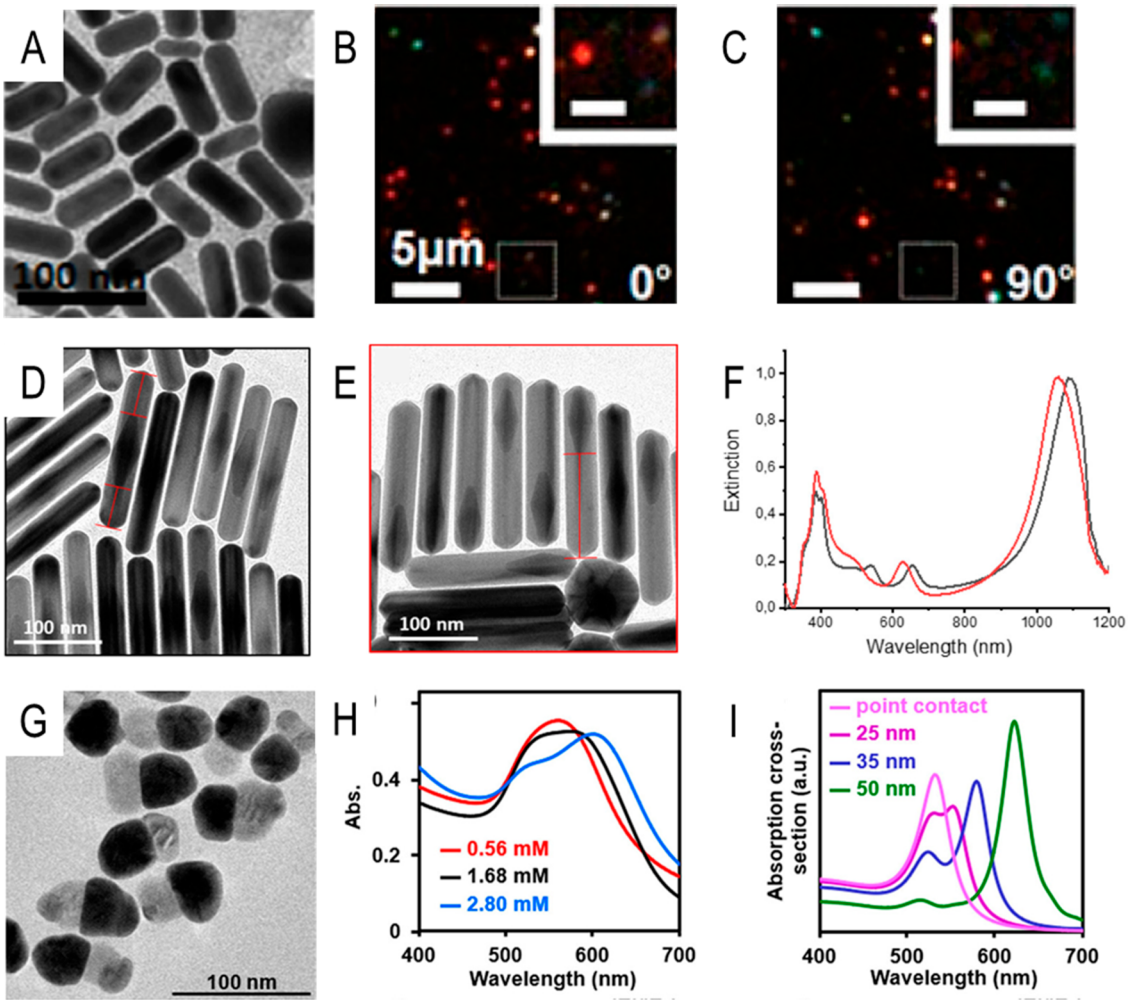

Figure 2. (A) TEM image of Au nanorods used in an example NP ink with corresponding optical microscopy images of dark-field scattering at (B) 0° and (C) 90° polarization. Inset scale bar is equal to 2 μm. TEM images of (D) centrosymmetric and (E) noncentrosymmetric Ag nanorods grown from Au bipyramidal seeds with (F) corresponding optical properties of parts D and E with the black trace corresponding to the centrosymmetric growth mode and the red trace corresponding to the noncentrosymmetric growth mode. (G) TEM image of Au-AgBr heterodimers with the (H) corresponding optical properties of Au-AgBr nanoparticles with concentration indicating changes in the amount of Ag precursor added. (I) FDTD-simulated optical properties of Au-AgBr heterodimers with varied sizes of the AgBr phase indicated in the legend; point contact refers to a 25 nm AgBr phase connected to Au via a single point. Parts A–C are adapted with permission from ref 26. Copyright 2021 American Chemical Society. Parts D–F are adapted with permission from ref 31. Copyright 2021 American Chemical Society. Parts G–I are adapted with permission from ref 56. Copyright 2020 Wiley-VCH Publishing.

For example, the galvanic replacement reaction on Ag–Pd heterodimers with Au (*i.e.,* a metal species with a higher reduction potential than those within the heterodimer) leads to an overall reduction in NP symmetry, from approximately C_{4v} to an approximate-C_1 symmetry.[47] Galvanic replacement of other multimetallic seeds is revealing generalizable pathways to complex heterostructures.[48]

As synthetic protocols expand, such symmetry-reduced nanostructures are revealing useful optical and catalytic properties that have yet to be fully explored or developed. To realize the potential of these new NPs, better understanding of the mechanisms for symmetry reduction are required. This insight should enable systematic variations in the composition and 3-D structure of metal NPs to fully reveal what application advances are possible. In the next two sections, evidence for the value of these new structures is presented in the context of their optical and catalytic properties.

OPTICAL PROPERTIES

Metal NPs can sustain localized surface plasmon resonances (LSPRs), where the electric field component of light interacts with the free electrons of the metal NP to give rise to a collective oscillation of electron density.[3,4,49,50] The specific wavelengths of light that can be scattered and absorbed by plasmonic metal NPs can be tuned through their composition and structure,[3,4] facilitating their use in security devices,[26,51] chemical sensors,[52] solar steam generators,[53] and more.[54] Notably, structures with reduced symmetry typically provide more plasmon modes compared to higher symmetry NPs, as the electron density can be polarized across the NP in different ways (recall the example of Au nanorods presented in the Introduction).[14]

The distinct LSPR response of NPs with lower symmetry oftentimes leads to a polarization dependence of the far-field response. For example, dark-field scattering from a single Au nanorod without polarization was shown to produce a red spot

https://doi.org/10.1021/acs.jpcc.1c07743
J. Phys. Chem. C 2021, 125, 23587–23596

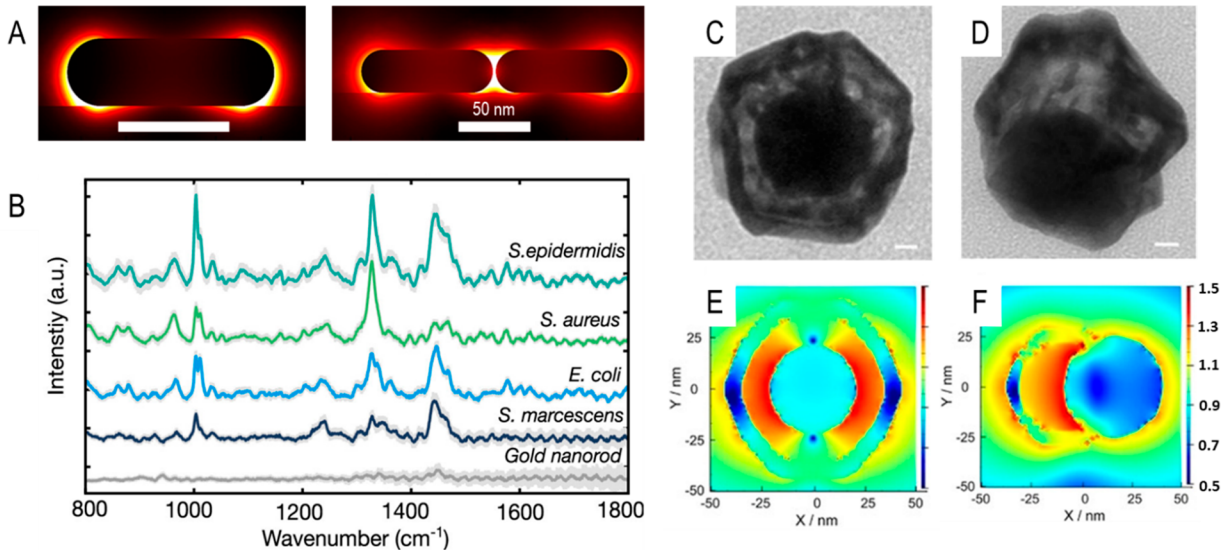

Figure 3. (A) Finite-element theoretical simulation of the local electric field for (left) single nanorods and (right) nanorod dimers. Scale bars 50 nm for both. (B) Liquid-SERS spectra for 675 nm nanorod solution (gray trace) and mixtures of different bacteria with nanorods (black, blue, green, and teal traces). TEM images of (C) concentric and (D) 50% coating with a hollow Au shell; scale bars 10 nm. FDTD calculated near-field EM intensity distribution for (E) concentric and (F) 50% coating with hollow Au shell structures indicating differences in EM field intensities for the different structures. Part A is adapted with permission from ref 63. Copyright 2016 American Chemical Society. Part B is adapted with permission from ref 64. Copyright 2020 American Chemical Society. Parts C−F are adapted with permission from ref 65. Copyright 2021 Wiley-VCH Publishing.

when imaged due the predominance of the longitudinal resonance; however, when excitation is parallel to the short axis, dark-field scattering produces a green spot.[26] Isotropic NPs do not show this effect.[26,55] This change in colorimetric response with polarization was used to create high encoding capacity security tags from dilute drop-castings of Au nanorods, which gave rise to random placement of the NPs on a tag surface. Shown in Figure 2A is a TEM image of Au nanorods. Figure 2B,C shows a photograph of the dark-field scattering from a dilute deposit of Au nanorods at 0 and 90° polarization. Notably, the observed color changes in response to the change in polarization, where the scattering pattern, the color responses, and polarization response can be used to authenticate the tag.[26]

The optical response of anisotropic NPs is also sensitive to compositional and architectural differences as the dielectric functions of both metals contribute to the optical response.[3] For example, the location of the metal seed in core@shell metal NPs can affect the LSPR.[15] Shown in Figure 2D,E are TEM images of Ag nanorods synthesized from Au nano-bipyramidal seeds by reducing $AgNO_3$ with ascorbic acid in the presence of cetyltrimethylammonium chloride.[31] The seeds can be positioned in a centrosymmetric manner, *i.e.*, D_{5h} symmetry versus noncentrosymmetric, *i.e.*, C_{5v} symmetry, respectively, depending on the presence of the cosolvent dimethyl sulfoxide (DMSO). Specifically, the NPs with noncentrosymmetric seeds were achieved by the addition of DMSO to the synthesis, which is hypothesized to disrupt the micellization of CTAC, causing the overgrowth of Ag to be restricted primarily to one side of the bipyramidal Au seed.[31] The LSPR of the NPs with noncentrosymmetric seeds was blue-shifted compared to the NPs with centrosymmetric seeds (Figure 2F).[31] This example highlights how changing the symmetry of core@shell NPs through the position of their seeds, the LSPR of metal NPs can be fine-tuned.

The use of heterodimers offers another type of symmetry-reduced NP with unique optical properties. The unique optical properties stem from the low symmetry of the NP system, with the second phase leading to a tunable LSPR. For example, the LSPR depends on the size, shape, and interface length of the heterodimer. The TEM of Au-AgBr heterodimer NPs (Figure 2G) shows the low symmetry nature of the heterodimer system (approximate $C_{\infty v}$symmetry) with phases distinguishable through Z-contrast.[56] The addition of the AgBr phase leads to the addition of a red-shifted LSPR peak through UV−visible spectroscopy, where the more Ag precursor added, the greater the red shift (Figure 2H).[56] The observed red shift was corroborated with finite-difference time-domain simulations (Figure 2I).[56] The multiple, tunable LSPR peaks arising from the different compositions of the heterodimer phases demonstrates the effectiveness of reduced-symmetry NPs toward manipulating the absorption and scattering properties of plasmonic NPs.

The optical near-field properties of metal NPs with reduced symmetry are promising for enhanced spectroscopies and sensing applications. Specifically, the electromagnetic field enhancement compared to the incident field is greatest at the plasmon resonance wavelength and can be used to enhance molecular signals.[54,57] These so-called hotspots (i.e., regions with strongly enhanced electric field) are present in symmetric NPs; however, the electromagnetic field enhancement of the hotspots can be greatly increased through the introduction of anisotropic features typical in symmetry reduction such as in nanorods and wires or in the sharp branches of nanostars.[58] The strongly enhanced electric field of these NPs can be used for surface-enhanced Raman scattering (SERS), where NPs that provide larger enhancement factors, such as rods, are better candidates for SERS applications regardless of molecular coverage.[59] In fact, the *E*-field enhancement at the tips of nanorods (Figure 3A, left) enables their use in monitoring reactions through SERS measurements, and the fabrication of

https://doi.org/10.1021/acs.jpcc.1c07743
J. Phys. Chem. C 2021, 125, 23587−23596

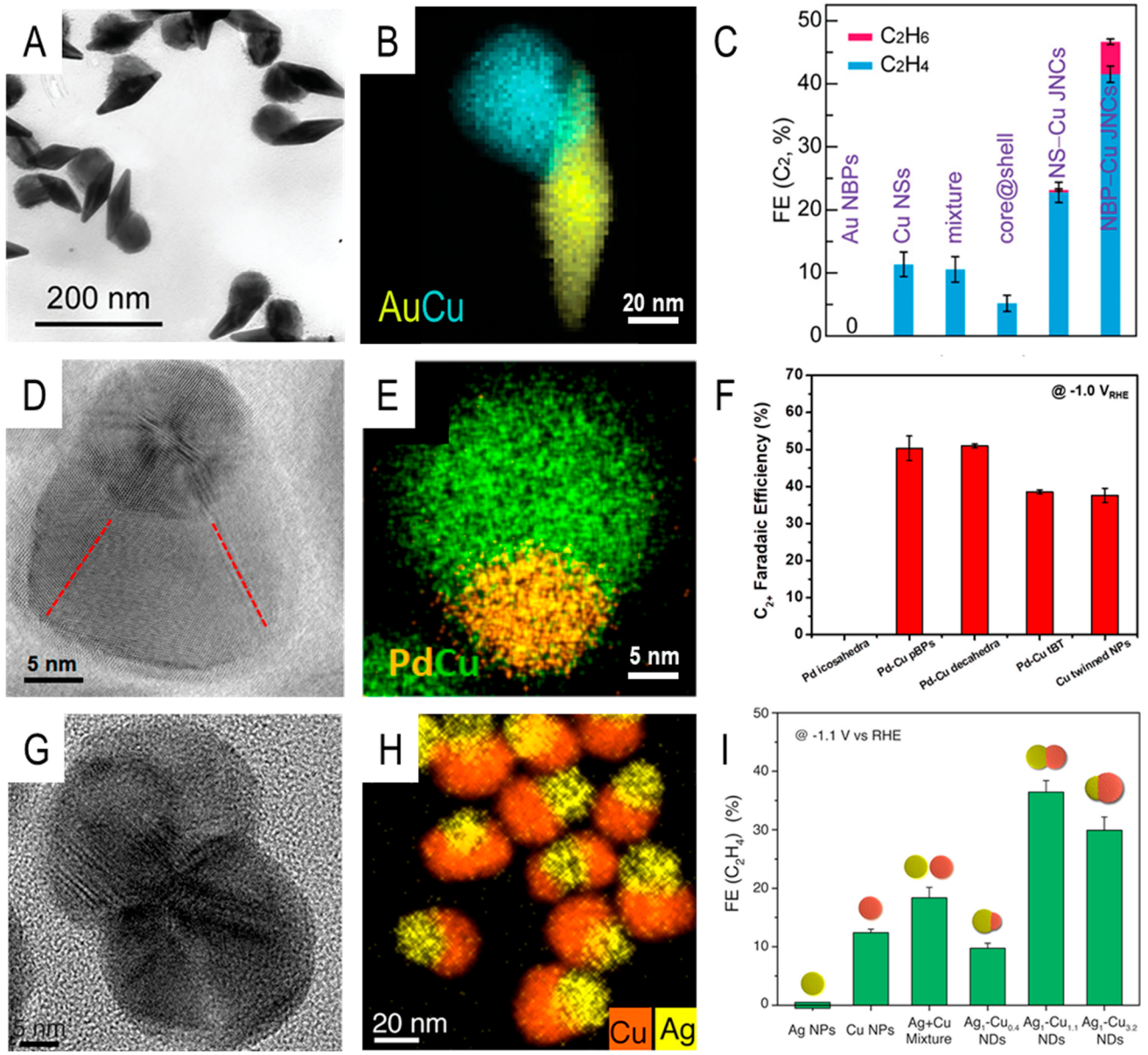

Figure 4. (A) Representative TEM image and (B) corresponding STEM-EDS elemental map of Au−Cu heterodimers grown from Au bipyramids (NBP-Cu JNCs). (C) Plot of faradaic efficiency for C_2 products for Au bipyramids, Cu nanospheres, Au@Cu nanospheres, Au nanosphere-Cu heterodimers, and Au bipyramid-Cu heterodimers showing enhanced product selectivity for C_2 products for the heterodimers. (D) TEM image and (E) corresponding STEM-EDS elemental map of Pd−Cu pentagonal bipyramids. Dashed red lines indicate twin planes. (F) Plot of C_2 product faradaic efficiency for Pd NPs, Pd−Cu heterodimers, and Cu NPs. (G) TEM image with (H) corresponding STEM-EDS of the 1:1.1 Ag−Cu heterodimers. (I) Plot of C_2 product selectivity for Ag NPs, Cu NPs, and Ag−Cu heterodimers showing domain size dependence for C_2 product selectivity. Parts A−C are adapted with permission from ref 28. Copyright 2021 Wiley-VCH Publishing. Parts D−F are adapted with permission from ref 69. Copyright 2020 American Chemical Society. Parts G−I are adapted with permission from ref 16. Copyright 2019 American Chemical Society.

SERS substrates as the enhancement factor increases for interparticle hot spots (Figure 3A, right).[59−64] In using approximately 670 nm Au nanorods mixed with *E. coli* under irradiation with a 785 nm incident laser, SERS detection of *E. coli* and other bacterial species was possible (Figure 3B).[64] Adding more complexity to NPs through symmetry reduction is an additional method for promising platforms for SERS. For example, a hollow Au shell on spherical Au seeds can be achieved through growing a silver shell on the exposed Au surface of a Au seed partially capped with a silica shell.[65] Following the deposition of Ag, galvanic replacement is used where Au replaces the Ag shell, forming a hollow Au shell.[65] Depending on the amount of surface coated in silica, the symmetry of the final product can be modified, with both concentric (quasi-D_∞ symmetry, Figure 3C) and 50% coating with the hollow shell (quasi-$C_{\infty v}$ symmetry, Figure 3D).[65] The difference in spatial symmetry, *i.e.*, D_∞ versus $C_{\infty v}$ allows for different ways for electron density to be polarized, yielding different hotspot generations (Figure 3E,F). The hotspot generation of the symmetry-reduced NPs could then be used for SERS detection of 4-MBN; however, the SERS signal could be further increased through linking the particles core-to-core, generating an intense hotspot in the interparticle gap.[65] These examples illustrate the increased capabilities of symmetry-

https://doi.org/10.1021/acs.jpcc.1c07743
J. Phys. Chem. C 2021, 125, 23587−23596

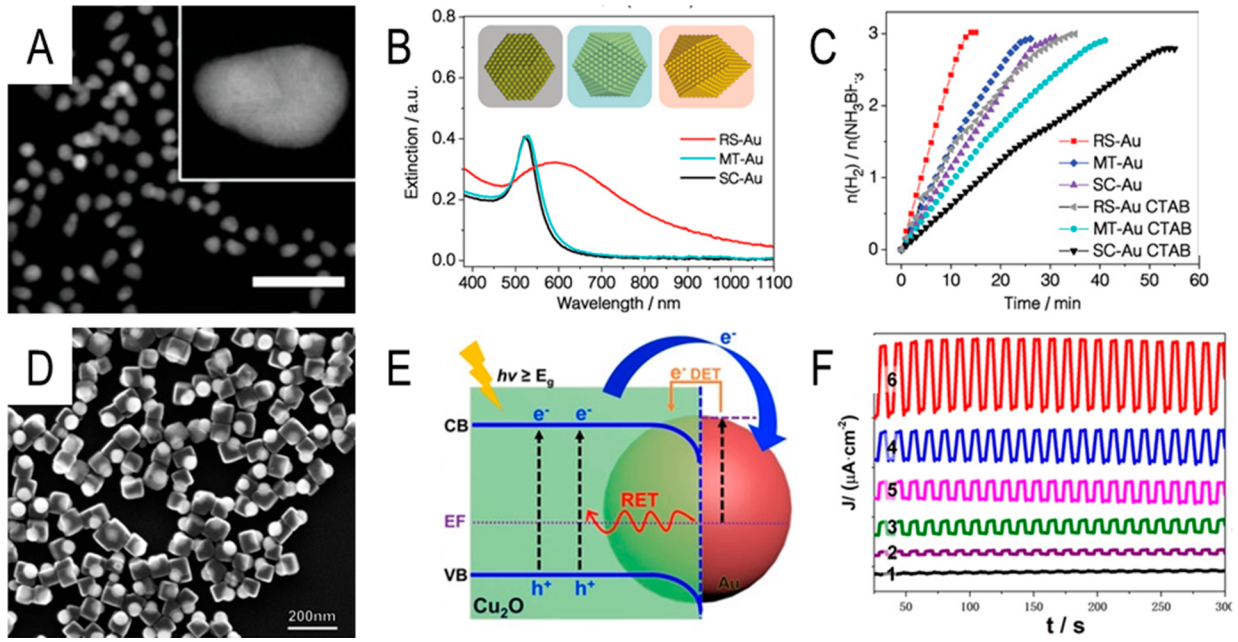

Figure 5. (A) Representative HAADF-STEM images of symmetry-reduced Au NPs grown from icosahedral Au seeds with (B) corresponding optical extinction for both symmetric and symmetry-reduced NPs showing a broad LSPR for the symmetry-reduced NPs; scale bar indicates 50 nm. (C) Time-dependent molar ratio of produced H_2 molecules to ammonia borane molecules for the hot electron-driven photocatalysis of ammonia borane hydrolysis with and without the presence of CTAB. (D) Representative SEM image of Au−Cu_2O with a (E) corresponding schematic illustrating the Schottky barrier present between the Au and Cu_2O phases in the Au−Cu_2O heterostructure. (F) Amperometric J−t curves of Au−Cu_2O NPs with octahedral Cu_2O domains (red), Au−Cu_2O NPs with cubic Cu_2O domains with 30 nm exposed Au surface (blue), 38 nm exposed Au surface (magenta), 11 nm exposed Au surface (green), Au@Cu_2O NPs (purple), and pure Cu_2O cubes (black). Parts A−C are adapted with permission from ref 70. Copyright 2020 Wiley-VCH Publishing. Parts D−F are adapted with permission from ref 72. Copyright 2020 Wiley-VCH Publishing.

reduced NPs for SERS; the ability to tune the LSPR maximum through NP symmetry facilitates the wavelength-dependent study of SERS.[63]

Taken together, the implementation of symmetry-reduced, anisotropic features leads to unique and tunable optoelectronic properties enabling applications in anticounterfeit devices and molecular sensing. Through synthetic control, it is possible to manipulate the overgrowth on seeds, leading to structures with reduced symmetry compared to the seed particles. These symmetry-reduced structures vary in form from nanorods to heterodimer-like structures and can have increased compositional complexity, all of which leads to different near- and far-field optoelectronic properties.

CATALYTIC PROPERTIES

A second area where symmetry-reduced NPs are finding use is as catalysts. NP catalysts make efficient use of precious materials given their high surface-to-volume ratios, with research over the past 10−20 years emphasizing how surface−adsorbate interactions (and in turn catalytic activity and selectivity) can be precisely tuned by selectively expressing specific facets via shape-controlled NPs.[7] Moreover, multimetallic NPs often display enhanced activity on account of ligand effects, particularly in alloy NPs.[66] Heterodimeric NPs are also being studied as catalysts due to the presence of multiple phases exposed to the surface, which have potential to provide unique interfacial reactivity as well as spillover effects.

The potential of heterodimeric NPs as catalysts was revealed through the study of Au−Cu NPs for electrocatalytic reduction of CO_2. Cu NPs have shown great promise as an electrocatalyst for CO_2 reduction, but poor selectivity persists.[67,68] To address this challenge, heterodimeric Au−Cu NPs were synthesized by overgrowth of Cu from bipyramidal Au seeds, where the large lattice mismatch between Au and Cu facilitated dimer formation (Figure 4A,B).[28] Au−Cu heterodimers from spherical Au seeds, core@shell Au@Cu NPs, Au nanobipyramids, Cu nanospheres, and mixtures of the two were also synthesized for comparison. The Au−Cu heterodimers, specifically the Au−Cu heterodimers grown from Au bipyramidal seeds, demonstrated the highest selectivity for C_2 products (Figure 4C).[28] The reduction in symmetry from seed (D_{5h}) to heterodimer (quasi-C_s) allows for the efficient conversion to C_2 products due to a tandem electrocatalysis pathway. The importance of symmetry is further shown through comparing the core@shell Au@Cu NPs (D_{5h} symmetry) to the heterodimer NPs (quasi-C_s symmetry), where the higher symmetry core@shell NPs had the worst selectivity toward C_2 products due to the lack of distinct Au and Cu domains at the NP surface.

In addition to the presence of distinct phases in heterodimers, the shape and size of the different domains are critical to tuning the electrocatalytic properties of these symmetry-reduced structures. For example, Pd−Cu heterostructures were found to have enhanced catalytic abilities toward the electrocatalytic reduction of CO_2 where C_2 products are favored.[69] Specifically, Cu was deposited on icosahedral Pd seeds in an aqueous solution of hexadecylamine, glucose, and Cu precursor, where the ratio of Cu precursor to hexadecylamine provided access to different NP shapes such as Pd−Cu pentagonal bipyramids (Figure 4D,E), decahedra, and truncated bitetrahedra.[69] The Pd−Cu NPs were compared to Pd icosahedra and Cu twinned NPs as

https://doi.org/10.1021/acs.jpcc.1c07743
J. Phys. Chem. C 2021, 125, 23587−23596

electrocatalysts for the CO_2 reduction reaction. The resulting Pd−Cu heterodimers, specifically the pentagonal bipyramids and decahedra (both approximate C_{5v} symmetry), demonstrated superior electrocatalytic performance in terms of C_2 product selectivity compared to pure Pd and pure Cu NPs.[69] Domain size is another crucial synthetic handle for achieving optimal selectivity in electrocatalysis. Manipulation of Cu domain size in Ag−Cu heterodimers was accomplished through varying the amount of Ag NP seeds added to an aqueous solution of hexadecylamine, Cu precursor, and ascorbic acid.[16] The obtained Ag−Cu heterodimers all had a similar reduction in symmetry compared to the Ag NP seeds (D_∞ symmetry to $C_{\infty v}$ symmetry); however, changing the volume of seeds added lead to different mass ratios of Ag/Cu (i.e., different sizes of Cu domains) of 1:0.4, 1:1.1 (Figure 4G,H), and 1:3.2.[16] In terms of product selectivity in the electrocatalytic CO_2 reduction reaction, the 1:1.1 mass ratio demonstrated the greatest faradaic efficiency compared to the other heterodimers and individual Ag and Cu NPs.[16] In both cases above, reduction in NP symmetry through the size and shape manipulation of heterodimer domains lead to increased selectivity for the electrocatalytic CO_2 reduction reaction.

In addition to electrocatalysis, photocatalysis can also provide a route to addressing the need for alternative energy sources. Photocatalysis relies on efficient light harvesting in which light is efficiently converted into useful energy to catalyze reactions and enhance charge separation. Efficient light harvesting can be achieved through broadband optical absorption, such as a broad absorption in LSPR. An example of such is through the symmetry reduction of Au icosahedral seeds through a cooperative overpotential and underpotential deposition strategy.[70] The reduction in symmetry from seed (I_h symmetry) to the resulting particle (quasi-C_{5v}, Figure 5A) led to a broadening of the plasmon band (Figure 5B), in which the resulting NPs had a significantly broadened LSPR compared to their more symmetric counterparts.[70] These broadband optical features make symmetry-reduced NPs attractive for photochemical reactions. Specifically, the symmetry-reduced NPs outperformed their more symmetric counterparts in terms of turnover frequency (Figure 5C) for the hot electron-driven photocatalysis of ammonia borane hydrolysis.[70] Specifically, the hydrolysis of ammonia borane was studied in which a xenon lamp illuminated the NPs in the presence of ammonia borane in which the symmetry-reduced NPs outperformed the more symmetric counterparts (Figure 5C) in terms of turnover frequency. The broadband optical properties of the symmetry-reduced NP system led to more efficient hot electron transfer than in highly symmetric NP systems, showing the promise of this class of NP in photocatalytic applications.

Another important aspect when considering photocatalytic applications is efficient charge separation. Coupling metals and semiconductors is known to promote charge separation due to a bending of the semiconductor conduction band at the metal−semiconductor interface, inhibiting the recombination of photogenerated charges known as the Schottky barrier.[71] Thus, research into the synthesis of hybrid NPs with both metal and semiconductor components became of interest to take advantage of this feature. However, core@shell metal@semiconductor NPs have a critical issue where charge accumulation greatly diminishes the photocurrent after a limit is reached. Interestingly, reducing the symmetry of the NP during the overgrowth of semiconductor material on metal seeds can overcome this issue. For example, the symmetry of Au@Cu_2O NPs could be tuned through modifying the concentration of 5-amino-2-mercaptobenzimi-dazole.[72] The change in capping ligand concentration led to either a full shell of Cu_2O to form in a cubic shape (O_h symmetry) or a Au−Cu_2O heterodimer NP (quasi-C_{4v} symmetry, Figure 5D) with varying amounts of Au exposed at the NP surface.[72] Interestingly, the symmetry-reduced NPs had more efficient charge separation in which photoexcited electrons flow from the Cu_2O to the Au domain (Figure 5E) and had higher photocurrents of up to 18 times the photocurrent of pure Cu_2O nanocubes (Figure 5F).[72] The highly symmetric core@shell structures had poor photocurrent generation due to the lack of Au and Cu_2O exposed at the surface compared to the symmetry-reduced Au−Cu_2O NPs.[72] This example highlights the potential of hybrid NPs composed of metal−semiconductor domains with reduced symmetry. Other hybrid NPs can be synthesized by depositing metal on semiconductor seeds (or vice versa) by leveraging the intrinsic differences in material class and judicious selection of reaction conditions, bringing together materials with different properties synergistically within one nanostructure.[73]

Overall, NPs with reduced symmetry display enhanced electro- and photocatalytic properties. Through using heterodimer particles, it is possible to increase the selectivity of electrocatalytic reactions with tandem catalysis. By finely tuning the size and shape of the different phases, these properties can be enhanced further. These symmetry-reduced NPs also demonstrate the ability to increase the efficiency of both light harvesting and charge separation, both of which are useful for photocatalysis.

CONCLUSIONS AND FUTURE OUTLOOK

Reduction in NP symmetry provides an efficient route to tailoring and enhancing properties at the nanoscale. Efforts in recent years have provided a variety of seed-mediated synthetic procedures in which the symmetry of the underlying seed is reduced relative to the final nanostructure on account of growth.[21,22] By precisely tuning the placement of atoms during growth to reduce NP symmetry, enhanced properties can be achieved for the NP systems. The reduced symmetry of the NP systems allows for greater tunability of near- and far-field optical properties yielding systems with specific absorption and scattering profiles. Additionally, this class of NPs enables enhanced activity and selectivity in electrochemical reactions, namely, the CO_2 reduction reaction as well as systems with enhanced light harvesting and charge separation capabilities for photocatalysis. Taken together, the reduction of NP symmetry provides unique and tunable properties at the nanoscale that are useful for optical and catalytic applications.

However, to take advantage of these interesting properties, a better understanding of symmetry-reduction mechanisms is required to better design syntheses with defined products in mind. For greater tunability of properties, synthetic routes toward symmetry-reduced structures with increasing architectural- and compositional-diversity are desired. Further, there is an impetus that must be placed on the ability to scale these types of syntheses up to provide larger quantities of symmetry-reduced NPs. In clearing up confusion about formation mechanisms, providing alternative routes to symmetry reduction for NPs with increasing architectural and compositional complexity and proposing reproducible methods for large quantities of symmetry-reduced NPs, a path can be made

https://doi.org/10.1021/acs.jpcc.1c07743
J. Phys. Chem. C 2021, 125, 23587−23596

to move the class of symmetry-reduced NPs from the lab to real world applications.

AUTHOR INFORMATION

Corresponding Author

Sara E. Skrabalak − *Department of Chemistry, Indiana University−Bloomington, Bloomington, Indiana 47405, United States;* orcid.org/0000-0002-1873-100X; Email: sskrabal@indiana.edu

Author

Zachary J. Woessner − *Department of Chemistry, Indiana University−Bloomington, Bloomington, Indiana 47405, United States*

Complete contact information is available at: https://pubs.acs.org/10.1021/acs.jpcc.1c07743

Author Contributions

The manuscript was written through contributions of all authors. All authors have given approval to the final version of the manuscript.

Notes

The authors declare no competing financial interest.

Biographies

Zachary J. Woessner is a Ph.D. candidate in the Skrabalak research group at Indiana University, Bloomington. He received his B.S. degree in chemistry from Westminster College in New Wilmington, Pennsylvania in 2017. Zach's current research is aimed at using different surface protecting groups to promote and study asymmetric branched nanostructures and studying their unique optoelectronic properties.

Sara E. Skrabalak completed her B.A. in Chemistry from Washington University in St. Louis and her Ph.D. in Chemistry from the University of Illinois at Urbana−Champaign. After postdoctoral research at the University of Washington−Seattle, Sara started as an Assistant Professor of Chemistry at Indiana University−Bloomington in 2008. She is currently the James H. Rudy Professor at Indiana University, having been recognized with numerous accolades. Professor Skrabalak began as Editor-in-Chief for both *Chemistry of Materials* and *ACS Materials Letters*. Her research group focuses on nanomaterial design and synthesis for diverse applications.

ACKNOWLEDGMENTS

This work was supported by U.S. NSF CHE No. 1904499 and Research Corporation for Science Advancement (2017 Frontiers in Research Excellence and Discovery Award).

REFERENCES

(1) Amendola, V.; Pilot, R.; Frasconi, M.; Maragò, O. M.; Iatì, M. A. Surface Plasmon Resonance in Gold Nanoparticles: a Review. *J. Phys.: Condens. Matter* **2017**, *29* (20), 203002.

(2) Chen, F.; Ehlerding, E. B.; Cai, W. Theranostic Nanoparticles. *J. Nucl. Med.* **2014**, *55* (12), 1919.

(3) Mayer, K. M.; Hafner, J. H. Localized Surface Plasmon Resonance Sensors. *Chem. Rev.* **2011**, *111* (6), 3828−3857.

(4) Willets, K. A.; Van Duyne, R. P. Localized Surface Plasmon Resonance Spectroscopy and Sensing. *Annu. Rev. Phys. Chem.* **2007**, *58* (1), 267−297.

(5) Camden, J. P.; Dieringer, J. A.; Zhao, J.; Van Duyne, R. P. Controlled Plasmonic Nanostructures for Surface-Enhanced Spectroscopy and Sensing. *Acc. Chem. Res.* **2008**, *41* (12), 1653−1661.

(6) Gilroy, K. D.; Ruditskiy, A.; Peng, H.-C.; Qin, D.; Xia, Y. Bimetallic Nanocrystals: Syntheses, Properties, and Applications. *Chem. Rev.* **2016**, *116* (18), 10414−10472.

(7) Shi, Y.; Lyu, Z.; Zhao, M.; Chen, R.; Nguyen, Q. N.; Xia, Y. Noble-Metal Nanocrystals with Controlled Shapes for Catalytic and Electrocatalytic Applications. *Chem. Rev.* **2021**, *121* (2), 649−735.

(8) Guntern, Y. T.; Okatenko, V.; Pankhurst, J.; Varandili, S. B.; Iyengar, P.; Koolen, C.; Stoian, D.; Vavra, J.; Buonsanti, R. Colloidal Nanocrystals as Electrocatalysts with Tunable Activity and Selectivity. *ACS Catal.* **2021**, *11* (3), 1248−1295.

(9) Carbone, L.; Cozzoli, P. D. Colloidal Heterostructured Nanocrystals: Synthesis and Growth Mechanisms. *Nano Today* **2010**, *5* (5), 449−493.

(10) Xia, Y.; Xiong, Y.; Lim, B.; Skrabalak, S. E. Shape-Controlled Synthesis of Metal Nanocrystals: Simple Chemistry Meets Complex Physics? *Angew. Chem., Int. Ed.* **2009**, *48* (1), 60−103.

(11) Wang, Y.; He, J.; Liu, C.; Chong, W. H.; Chen, H. Thermodynamics versus Kinetics in Nanosynthesis. *Angew. Chem., Int. Ed.* **2015**, *54* (7), 2022−2051.

(12) Verlhac, M.-H.; Lefebvre, C.; Guillaud, P.; Rassinier, P.; Maro, B. Asymmetric Division in Mouse Oocytes: with or without Mos. *Curr. Biol.* **2000**, *10* (20), 1303−1306.

(13) Chen, H.; Shao, L.; Li, Q.; Wang, J. Gold Nanorods and their Plasmonic Properties. *Chem. Soc. Rev.* **2013**, *42* (7), 2679−2724.

(14) Cao, J.; Sun, T.; Grattan, K. T. V. Gold Nanorod-Based Localized Surface Plasmon Resonance Biosensors: A Review. *Sens. Actuators, B* **2014**, *195*, 332−351.

(15) Zhu, C.; Zeng, J.; Tao, J.; Johnson, M. C.; Schmidt-Krey, I.; Blubaugh, L.; Zhu, Y.; Gu, Z.; Xia, Y. Kinetically Controlled Overgrowth of Ag or Au on Pd Nanocrystal Seeds: From Hybrid Dimers to Nonconcentric and Concentric Bimetallic Nanocrystals. *J. Am. Chem. Soc.* **2012**, *134* (38), 15822−15831.

(16) Huang, J.; Mensi, M.; Oveisi, E.; Mantella, V.; Buonsanti, R. Structural Sensitivities in Bimetallic Catalysts for Electrochemical CO2 Reduction Revealed by Ag−Cu Nanodimers. *J. Am. Chem. Soc.* **2019**, *141* (6), 2490−2499.

(17) Zheng, Z.; Tachikawa, T.; Majima, T. Plasmon-Enhanced Formic Acid Dehydrogenation Using Anisotropic Pd−Au Nanorods Studied at the Single-Particle Level. *J. Am. Chem. Soc.* **2015**, *137* (2), 948−957.

(18) Zheng, Z.; Tachikawa, T.; Majima, T. Single-Particle Study of Pt-Modified Au Nanorods for Plasmon-Enhanced Hydrogen Generation in Visible to Near-Infrared Region. *J. Am. Chem. Soc.* **2014**, *136* (19), 6870−6873.

(19) Ma, S.; Sadakiyo, M.; Heima, M.; Luo, R.; Haasch, R. T.; Gold, J. I.; Yamauchi, M.; Kenis, P. J. A. Electroreduction of Carbon Dioxide to Hydrocarbons Using Bimetallic Cu−Pd Catalysts with Different Mixing Patterns. *J. Am. Chem. Soc.* **2017**, *139* (1), 47−50.

(20) Xia, Y.; Gilroy, K. D.; Peng, H.-C.; Xia, X. Seed-Mediated Growth of Colloidal Metal Nanocrystals. *Angew. Chem., Int. Ed.* **2017**, *56* (1), 60−95.

(21) Gilroy, K. D.; Peng, H.-C.; Yang, X.; Ruditskiy, A.; Xia, Y. Symmetry Breaking during Nanocrystal Growth. *Chem. Commun.* **2017**, *53* (33), 4530−4541.

(22) Huang, Z.; Gong, J.; Nie, Z. Symmetry-Breaking Synthesis of Multicomponent Nanoparticles. *Acc. Chem. Res.* **2019**, *52* (4), 1125−1133.

(23) Weiner, R. G.; Kunz, M. R.; Skrabalak, S. E. Seeding a New Kind of Garden: Synthesis of Architecturally Defined Multimetallic Nanostructures by Seed-Mediated Co-Reduction. *Acc. Chem. Res.* **2015**, *48* (10), 2688−2695.

(24) Skrabalak, S. E. Symmetry in Seeded Metal Nanocrystal Growth. *Acc. Mater. Res.* **2021**, *2* (8), 621−629.

(25) Smith, J. D.; Scanlan, M. M.; Chen, A. N.; Ashberry, H. M.; Skrabalak, S. E. Kinetically Controlled Sequential Seeded Growth: A General Route to Crystals with Different Hierarchies. *ACS Nano* **2020**, *14* (11), 15953−15961.

(26) Smith, J. D.; Reza, M. A.; Smith, N. L.; Gu, J.; Ibrar, M.; Crandall, D. J.; Skrabalak, S. E. Plasmonic Anticounterfeit Tags with

High Encoding Capacity Rapidly Authenticated with Deep Machine Learning. *ACS Nano* **2021**, *15* (2), 2901−2910.
(27) Ibrar, M.; Skrabalak, S. E. Designer Plasmonic Nanostructures for Unclonable Anticounterfeit Tags. *Small Struct.* **2021**, *2*, 2100043.
(28) Jia, H.; Yang, Y.; Chow, T. H.; Zhang, H.; Liu, X.; Wang, J.; Zhang, C.-y. Symmetry-Broken Au−Cu Heterostructures and their Tandem Catalysis Process in Electrochemical CO2 Reduction. *Adv. Funct. Mater.* **2021**, *31* (27), 2101255.
(29) González-Rubio, G.; Kumar, V.; Llombart, P.; Díaz-Núñez, P.; Bladt, E.; Altantzis, T.; Bals, S.; Peña-Rodríguez, O.; Noya, E. G.; MacDowell, L. G.; et al. Disconnecting Symmetry Breaking from Seeded Growth for the Reproducible Synthesis of High Quality Gold Nanorods. *ACS Nano* **2019**, *13* (4), 4424−4435.
(30) Walsh, M. J.; Tong, W.; Katz-Boon, H.; Mulvaney, P.; Etheridge, J.; Funston, A. M. A Mechanism for Symmetry Breaking and Shape Control in Single-Crystal Gold Nanorods. *Acc. Chem. Res.* **2017**, *50* (12), 2925−2935.
(31) Goldmann, C.; De Frutos, M.; Hill, E. H.; Constantin, D.; Hamon, C. Symmetry Breaking in Seed-Mediated Silver Nanorod Growth Induced by Dimethyl Sulfoxide. *Chem. Mater.* **2021**, *33* (8), 2948−2956.
(32) Chen, T.; Chen, G.; Xing, S.; Wu, T.; Chen, H. Scalable Routes to Janus Au−SiO2 and Ternary Ag−Au−SiO2 Nanoparticles. *Chem. Mater.* **2010**, *22* (13), 3826−3828.
(33) Qiu, J.; Xie, M.; Lyu, Z.; Gilroy, K. D.; Liu, H.; Xia, Y. General Approach to the Synthesis of Heterodimers of Metal Nanoparticles through Site-Selected Protection and Growth. *Nano Lett.* **2019**, *19* (9), 6703−6708.
(34) Wang, Z.; He, B.; Xu, G.; Wang, G.; Wang, J.; Feng, Y.; Su, D.; Chen, B.; Li, H.; Wu, Z.; et al. Transformable Masks for Colloidal Nanosynthesis. *Nat. Commun.* **2018**, *9* (1), 563.
(35) Feng, S.; Song, X.; Xu, Q.; Shen, X.; Xu, J.; Chen, H. A General Approach for Encapsulating Nanoparticles by Polystyrene-block-poly(acrylic acid) Shell in Colloidal. *J. Phys. Chem. Solids* **2019**, *135*, 109019.
(36) Jiang, T.; Chen, G.; Tian, X.; Tang, S.; Zhou, J.; Feng, Y.; Chen, H. Construction of Long Narrow Gaps in Ag Nanoplates. *J. Am. Chem. Soc.* **2018**, *140* (46), 15560−15563.
(37) Golze, S. D.; Porcu, S.; Zhu, C.; Sutter, E.; Ricci, P. C.; Kinzel, E. C.; Hughes, R. A.; Neretina, S. Sequential Symmetry-Breaking Events as a Synthetic Pathway for Chiral Gold Nanostructures with Spiral Geometries. *Nano Lett.* **2021**, *21* (7), 2919−2925.
(38) Peng, H.-C.; Park, J.; Zhang, L.; Xia, Y. Toward a Quantitative Understanding of Symmetry Reduction Involved in the Seed-Mediated Growth of Pd Nanocrystals. *J. Am. Chem. Soc.* **2015**, *137* (20), 6643−6652.
(39) Chen, A. N.; Scanlan, M. M.; Skrabalak, S. E. Surface Passivation and Supersaturation: Strategies for Regioselective Deposition in Seeded Syntheses. *ACS Nano* **2017**, *11* (12), 12624−12631.
(40) Zeng, J.; Zhu, C.; Tao, J.; Jin, M.; Zhang, H.; Li, Z.-Y.; Zhu, Y.; Xia, Y. Controlling the Nucleation and Growth of Silver on Palladium Nanocubes by Manipulating the Reaction Kinetics. *Angew. Chem., Int. Ed.* **2012**, *51* (10), 2354−2358.
(41) Liu, G.; Zhang, C.; Wu, J.; Mirkin, C. A. Using Scanning-Probe Block Copolymer Lithography and Electron Microscopy To Track Shape Evolution in Multimetallic Nanoclusters. *ACS Nano* **2015**, *9* (12), 12137−12145.
(42) Hajfathalian, M.; Gilroy, K. D.; Hughes, R. A.; Neretina, S. Citrate-Induced Nanocubes: A Re-Examination of the Role of Citrate as a Shape-Directing Capping Agent for Ag-Based Nanostructures. *Small* **2016**, *12* (25), 3444−3452.
(43) Gu, H.; Yang, Z.; Gao, J.; Chang, C. K.; Xu, B. Heterodimers of Nanoparticles: Formation at a Liquid−Liquid Interface and Particle-Specific Surface Modification by Functional Molecules. *J. Am. Chem. Soc.* **2005**, *127* (1), 34−35.
(44) Zhang, X.; Fu, Q.; Duan, H.; Song, J.; Yang, H. Janus Nanoparticles: From Fabrication to (Bio)Applications. *ACS Nano* **2021**, *15* (4), 6147−6191.
(45) Zhang, L.; Wang, Y.; Tong, L.; Xia, Y. Synthesis of Colloidal Metal Nanocrystals in Droplet Reactors: The Pros and Cons of Interfacial Adsorption. *Nano Lett.* **2014**, *14* (7), 4189−4194.
(46) Jin, M.; Zhang, H.; Wang, J.; Zhong, X.; Lu, N.; Li, Z.; Xie, Z.; Kim, M. J.; Xia, Y. Copper Can Still Be Epitaxially Deposited on Palladium Nanocrystals To Generate Core−Shell Nanocubes Despite Their Large Lattice Mismatch. *ACS Nano* **2012**, *6* (3), 2566−2573.
(47) Chen, A. N.; McClain, S. M.; House, S. D.; Yang, J. C.; Skrabalak, S. E. Mechanistic Study of Galvanic Replacement of Chemically Heterogeneous Templates. *Chem. Mater.* **2019**, *31* (4), 1344−1351.
(48) Chen, A. N.; Endres, E. J.; Ashberry, H. M.; Bueno, S. L. A.; Chen, Y.; Skrabalak, S. E. Galvanic Replacement of Intermetallic Nanocrystals as a Route Toward Complex Heterostructures. *Nanoscale* **2021**, *13* (4), 2618−2625.
(49) Myroshnychenko, V.; Rodríguez-Fernández, J.; Pastoriza-Santos, I.; Funston, A. M.; Novo, C.; Mulvaney, P.; Liz-Marzán, L. M.; García de Abajo, F. J. Modelling the Optical Response of Gold Nanoparticles. *Chem. Soc. Rev.* **2008**, *37* (9), 1792−1805.
(50) Hutter, E.; Fendler, J. H. Exploitation of Localized Surface Plasmon Resonance. *Adv. Mater.* **2004**, *16* (19), 1685−1706.
(51) Smith, A. F.; Skrabalak, S. E. Metal Nanomaterials for Optical Anti-Counterfeit Labels. *J. Mater. Chem. C* **2017**, *5* (13), 3207−3215.
(52) Woessner, Z. J.; Chen, A. N.; Skrabalak, S. E. Importance of Pd Distribution to Au−Pd Nanocrystals with High Refractive Index Sensitivity. *J. Phys. Chem. C* **2021**, *125* (20), 11262−11270.
(53) Wang, X.; He, Y.; Liu, X.; Shi, L.; Zhu, J. Investigation of Photothermal Heating Enabled by Plasmonic Nanofluids for Direct Solar Steam Generation. *Sol. Energy* **2017**, *157*, 35−46.
(54) Wang, L.; Hasanzadeh Kafshgari, M.; Meunier, M. Optical Properties and Applications of Plasmonic-Metal Nanoparticles. *Adv. Funct. Mater.* **2020**, *30* (51), 2005400.
(55) Smith, A. F.; Patton, P.; Skrabalak, S. E. Plasmonic Nanoparticles as a Physically Unclonable Function for Responsive Anti-Counterfeit Nanofingerprints. *Adv. Funct. Mater.* **2016**, *26* (9), 1315−1321.
(56) Takahashi, R.; Fujishima, M.; Tada, H.; Soejima, T. Symmetry Breaking Induced by Growth Kinetics: One-Pot Synthesis of Janus Au−AgBr Nanoparticles. *ChemNanoMat* **2020**, *6* (10), 1485−1495.
(57) Langer, J.; Jimenez de Aberasturi, D.; Aizpurua, J.; Alvarez-Puebla, R. A.; Auguié, B.; Baumberg, J. J.; Bazan, G. C.; Bell, S. E. J.; Boisen, A.; Brolo, A. G.; et al. Present and Future of Surface-Enhanced Raman Scattering. *ACS Nano* **2020**, *14* (1), 28−117.
(58) Smith, J. D.; Woessner, Z. J.; Skrabalak, S. E. Branched Plasmonic Nanoparticles with High Symmetry. *J. Phys. Chem. C* **2019**, *123* (30), 18113−18123.
(59) Solís, D. M.; Taboada, J. M.; Obelleiro, F.; Liz-Marzán, L. M.; García de Abajo, F. J. Optimization of Nanoparticle-Based SERS Substrates through Large-Scale Realistic Simulations. *ACS Photonics* **2017**, *4* (2), 329−337.
(60) Rodal-Cedeira, S.; Montes-García, V.; Polavarapu, L.; Solís, D. M.; Heidari, H.; La Porta, A.; Angiola, M.; Martucci, A.; Taboada, J. M.; Obelleiro, F.; et al. Plasmonic Au@Pd Nanorods with Boosted Refractive Index Susceptibility and SERS Efficiency: A Multifunctional Platform for Hydrogen Sensing and Monitoring of Catalytic Reactions. *Chem. Mater.* **2016**, *28* (24), 9169−9180.
(61) Tian, X.-D.; Lin, Y.; Dong, J.-C.; Zhang, Y.-J.; Wu, S.-R.; Liu, S.-Y.; Zhang, Y.; Li, J.-F.; Tian, Z.-Q. Synthesis of Ag Nanorods with Highly Tunable Plasmonics toward Optimal Surface-Enhanced Raman Scattering Substrates Self-Assembled at Interfaces. *Adv. Opt. Mater.* **2017**, *5* (21), 1700581.
(62) Serrano-Montes, A. B.; Jimenez de Aberasturi, D.; Langer, J.; Giner-Casares, J. J.; Scarabelli, L.; Herrero, A.; Liz-Marzán, L. M. A General Method for Solvent Exchange of Plasmonic Nanoparticles and Self-Assembly into SERS-Active Monolayers. *Langmuir* **2015**, *31* (33), 9205−9213.
(63) Lin, K.-Q.; Yi, J.; Hu, S.; Liu, B.-J.; Liu, J.-Y.; Wang, X.; Ren, B. Size Effect on SERS of Gold Nanorods Demonstrated via Single

Nanoparticle Spectroscopy. *J. Phys. Chem. C* **2016**, *120* (37), 20806−20813.
(64) Tadesse, L. F.; Ho, C.-S.; Chen, D.-H.; Arami, H.; Banaei, N.; Gambhir, S. S.; Jeffrey, S. S.; Saleh, A. A. E.; Dionne, J. Plasmonic and Electrostatic Interactions Enable Uniformly Enhanced Liquid Bacterial Surface-Enhanced Raman Scattering (SERS). *Nano Lett.* **2020**, *20* (10), 7655−7661.
(65) Zhu, R.; Feng, H.; Li, Q.; Su, L.; Fu, Q.; Li, J.; Song, J.; Yang, H. Asymmetric Core−Shell Gold Nanoparticles and Controllable Assemblies for SERS Ratiometric Detection of MicroRNA. *Angew. Chem., Int. Ed.* **2021**, *60* (22), 12560−12568.
(66) Bueno, S. L. A.; Ashberry, H. M.; Shafei, I.; Skrabalak, S. E. Building Durable Multimetallic Electrocatalysts from Intermetallic Seeds. *Acc. Chem. Res.* **2021**, *54* (7), 1662−1672.
(67) Reske, R.; Mistry, H.; Behafarid, F.; Roldan Cuenya, B.; Strasser, P. Particle Size Effects in the Catalytic Electroreduction of CO2 on Cu Nanoparticles. *J. Am. Chem. Soc.* **2014**, *136* (19), 6978−6986.
(68) Wakerley, D.; Lamaison, S.; Ozanam, F.; Menguy, N.; Mercier, D.; Marcus, P.; Fontecave, M.; Mougel, V. Bio-inspired Hydrophobicity Promotes CO2 Reduction on a Cu Surface. *Nat. Mater.* **2019**, *18* (11), 1222−1227.
(69) Lyu, Z.; Zhu, S.; Xu, L.; Chen, Z.; Zhang, Y.; Xie, M.; Li, T.; Zhou, S.; Liu, J.; Chi, M.; et al. Kinetically Controlled Synthesis of Pd−Cu Janus Nanocrystals with Enriched Surface Structures and Enhanced Catalytic Activities toward CO2 Reduction. *J. Am. Chem. Soc.* **2021**, *143* (1), 149−162.
(70) Shao, W.; Pan, Q.; Chen, Q.; Zhu, C.; Tao, W.; Zhu, H.; Song, H.; Liu, X.; Tan, P.-H.; Sheng, G.; et al. Symmetry Breaking in Monometallic Nanocrystals toward Broadband and Direct Electron Transfer Enhanced Plasmonic Photocatalysis. *Adv. Funct. Mater.* **2021**, *31* (3), 2006738.
(71) Liu, X.; Iocozzia, J.; Wang, Y.; Cui, X.; Chen, Y.; Zhao, S.; Li, Z.; Lin, Z. Noble Metal−Metal Oxide Nanohybrids with Tailored Nanostructures for Efficient Solar Energy Conversion, Photocatalysis and Environmental Remediation. *Energy Environ. Sci.* **2017**, *10* (2), 402−434.
(72) Xu, W.; Jia, J.; Wang, T.; Li, C.; He, B.; Zong, J.; Wang, Y.; Fan, H. J.; Xu, H.; Feng, Y.; Chen, H. Continuous Tuning of Au−Cu2O Janus Nanostructures for Efficient Charge Separation. *Angew. Chem., Int. Ed.* **2020**, *59* (49), 22246−22251.
(73) Mishra, N. Metal−Semiconductor Hybrid Nano-Heterostructures for Photocatalysis Application. In *Semiconductor Photocatalysis−Materials, Mechanisms and Applications*; IntechOpen, 2016, DOI: 10.5772/62636.

https://doi.org/10.1021/acs.jpcc.1c07743
J. Phys. Chem. C 2021, 125, 23587−23596